192 (2024) 206965

Contents lists available at ScienceDirect

Applied Catalysis O: Open

journal homepage: www.elsevier.com/locate/apcato

Boosting light-driven hydrogen evolution through cerium vanadate/cerium sulphide type–II heterostructure

K. Yogesh Kumar [a], M.K. Prashanth [b], L. Parashuram [c], H. Shanavaz [a], C.B. Pradeep Kumar [d], Fahd Alharethy [e], Byong-Hun Jeon [f,*], K.K. Prashanth [g], M.S. Raghu [h,*]

[a] Department of Chemistry, Faculty of Engineering and Technology, Jain University, Bangalore 562112, India
[b] Department of Chemistry, BNM Institute of Technology, Banashankari, Bangalore 560070, India
[c] Department of Chemistry, Nitte Meenakshi Institute of Technology, Yelahanka, Bangalore 560064, India
[d] Department of Chemistry, Malnad College of Engineering, Hassan, India
[e] Department of Chemistry, College of Science, King Saud University, 11451 Riyadh, Saudi Arabia
[f] Department of Earth Resources and Environmental Engineering, Hanyang University, 222, Wangsimni-ro, Seongdong-gu, Seoul 04763, Republic of Korea
[g] Department of Mathematics, New Horizon College of Engineering, Outer Ring Road, Bangalore, 560103, India
[h] Department of Chemistry, New Horizon College of Engineering, Outer Ring Road, Bangalore, 560103, India

ARTICLE INFO

Keywords:
$CeVO_4$
Ce_2S_3
Photochemical
Photoelectrochemical
H_2 evolution

ABSTRACT

Fabrication of heterostructures to boost the light-driven hydrogen evolution is one of the efficient way to address the energy crisis across the globe. Cerium vanadate (CeV)/Cerium sulphide (CeS) heterostructure has been synthesized using a simple hydrothermal method. Structural, spectroscopic, morphological, optical and photoelectrochemical characterizations confirm the formation of heterostructure between CeV and CeS. Photochemical hydrogen evolution was observed in all the three catalysts (CeV, CeS and CeV/CeS) both under visible and ultraviolet light sources. CeS, CeV and CeV/CeS found to evolve 3897, 6453 and 12,456 μmol of hydrogen in 4 h, respectively under visible light. In addition photoelectrochemical hydrogen evolution experiment was conducted in which, CeV/CeS heterostructure showed high photocurrent density at 0.25 V vs. RHE, which is almost 1.47 folds greater than that of CeV and 2.1 times that of CeS. The optical and electrochemical characteristics shows that photocatalytic hydrogen evolution follows type-II heterostructure. A good stability of the CeV/CeS heterostructure finds its suitability for practical applications for various photocatalytic experiments.

1. Introduction

The evolution of hydrogen is critical in many fields due to its ability to address serious global concerns and support sustainable development [1,2]. Hydrogen is a clean energy carrier that, when used in fuel cells, combustion engines, or as a feedstock for chemical processes, emits only water vapour as a byproduct, making it critical for decreasing greenhouse gas emissions and fighting climate change [3–5]. When energy demand is high or renewable energy generation is low, we can convert this stored hydrogen back into electricity or use it as a fuel, thereby improving grid stability and reliability. Hydrogen fuel cells are a possible solution for zero-emission transportation in cars, buses, trucks, and even trains [6,7]. The evolution of hydrogen permits the generation of clean energy for transportation, lowering air pollution and reliance on fossil fuels. Research and development in hydrogen evolution mainly involve electrocatalytic, photochemical, and photoelectrochemical techniques [8,9]. Hydrogen evolution is widely achieved using costly metals like Pt, Pd, and Ru through electrochemical techniques. Light-driven H_2 evolution is a viable avenue for sustainable hydrogen synthesis, with various advantages over electrochemical approaches, particularly in terms of using renewable energy sources and reducing environmental effects [10–12].

Photochemical/electrochemical hydrogen evolution reactions depend mainly on the bandgap, structure, defects, light assimilation, and flat band potentials of the catalyst [13–15]. Rare earth metal vanadates have been used for various photocatalytic and other catalytic applications [16–18]. $CeVO_4$ (CeV) is one such bimetallic oxide projecting its semiconductor characteristics with a bandgap of 2 to 2.6 eV. CeV's remarkable redox and optical capabilities as a catalyst are due to the multiple electronic transitions of its constituent lanthanides and its

* Corresponding authors.
E-mail addresses: bhjeon@hanyang.ac.kr (B.-H. Jeon), dr.msraghu@newhorizonindia.edu (M.S. Raghu).

https://doi.org/10.1016/j.apcato.2024.206965
Received 27 March 2024; Received in revised form 5 June 2024; Accepted 7 June 2024
Available online 8 June 2024

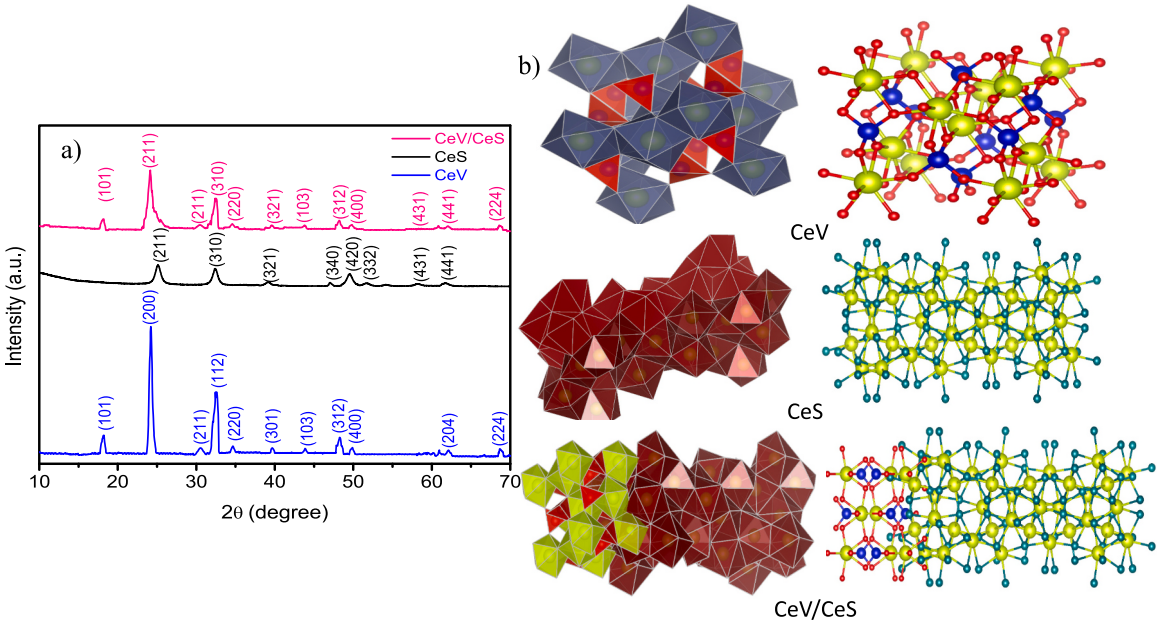

Fig. 1. 1a) The X-ray diffraction patterns of CeV, CeS and CeV/CeS and 1b) Crystal structure of CeV, CeS and CeV/CeS.

partially filled 4f electronic structure [19,20]. The bandgap of CeV indicates its ability to absorb light in both ultraviolet (UV) and visible regions. It is reported that, the coexistence of oxidation states (Ce^{4+} and Ce^{3+} ions) on the surface of CeV nanostructures acts as the major catalytic centre and is expected to exhibit superior photocatalytic activity [21–23]. The reduction of Ce^{4+} to Ce^{3+} is possible due to the difference in the energy levels of V 3d and Ce 4f orbitals. The V^{5+} species remain stable in the redox cycle due to their higher 3d energy levels, which work with the O 2p states of the VO_4^{3-} ions to form bandgap states. CeV has been explored in various applications like sensors, photocatalysis, batteries, and other energy storage devices [23–25]. Even though CeV possesses these properties, its photocatalytic efficiency is found to be low due to the fast recombination of photo-induced electrons and holes and its low conductivity. Hence, it is preferred to combine it with other carbonaceous materials or semiconductors that lead to the generation of composites or heterostructures of various types depending on the edge potentials, conductivity, and bandgap [26,27].

Cerium's combination with sulphur metal, Ce_2S_3 (CeS), shows a wide photoresponse range and rapid charge carrier dynamics because of the less positive valence band filled by S 3p orbitals [28,29]. A bandgap of ~2.1 eV in the in the high negative conduction band of CeS has found applications in photocatalytic degradation of pollutants, sensors, and optoelectronic devices [30]. Though it has the ability to absorb light in a wide range, its efficiency in photocatalysis is not as expected. The reason could be the fast recombination of electrons and holes and photocorrosion during redox reactions [31]. Therefore, it is desirable to combine it with other light-active materials to boost the photocatalytic activities.

Combining the best properties of CeV and CeS that result in heterostructure could be an alternate way to resolve the issues associated with individual materials. Several researchers showed that type-II heterostructures could accomplish active spatial separation under light irradiation effectively compared to other types of heterostructures.

The authors of the present work have executed the work consisting of the formation of type-II heterostructure between CeV and CeS using hydrothermal method. The synthetic procedure is found to be simple, facile and economical in nature. The combined form of CeV and CeS have not been explored irrespective of their upright semiconductor characteristics. Synthesized catalysts (CeV, CeS and CeV/CeS) were used for photocatalytic hydrogen evolution in the presence of a sacrificial agent using both UV and visible light sources. In addition, FTO substrate have been fabricated using these materials and the photoelectrochemical hydrogen evolution has been examined using an electrochemical workstation with a three-electrode system. In both cases, CeV/CeS had better hydrogen evolution than the individual materials because type-II heterostructures were formed. This work may help the researchers explore more combinations of metal vanadates and metal sulphides for effective light driven applications.

2. Experimental

2.1. Materials

$Ce(NO_3)_3$, Na_2S_3, $NaVO_3$, NH_4OH, C_2H_5OH and all sacrificial agents were procured from Merck India Pvt., Ltd., Mumbai India. All the chemicals are of analytical grade and used as such. Distilled water was used to prepare reagents and other studies.

2.2. Synthesis of CeV, CeS and CeV/CeS

In two separate beakers, labelled A and B, 50 mL of a $Ce(NO_3)_3$ solution with a concentration of 0.1 M was taken. Pour 50 mL of a 0.1 M Na_2S_3 solution into Beaker A, and then add a drop of a 1:1 ratio of $NaVO_3$ and NH_4OH to Beaker B. After mixing the two solutions, we subjected them to ultrasonication for 30 min. After that, the entire reaction mixture is transferred to a 200 mL Teflon-lined stainless steel hydrothermal bomb and heated at 130° for 6 h. The mixture was allowed to cool, filtered, and washed several times with water and ethanol. The hot air oven was set to 80 °C and dried the filtrate overnight. CeV and CeS samples were prepared individually for comparison using the same procedure, but without combining them.

2.3. Photochemical/electrochemical hydrogen evolution

The hydrogen evolution reaction was carried out using a 300 W Xe lamp (7658 lm; 95 mW cm^{-2}) as a visible light source and 250 W mercury vapour lamp (10,845 lm; 85 mW cm^{-2}) as a UV light source. Exactly 25 mg of the synthesized catalysts, CeS, CeV and CeV/CeS were taken in a clean quartz round-bottom flask containing 50 mL of water. A sacrificial agent (20 mL) was added to the solution and purged with

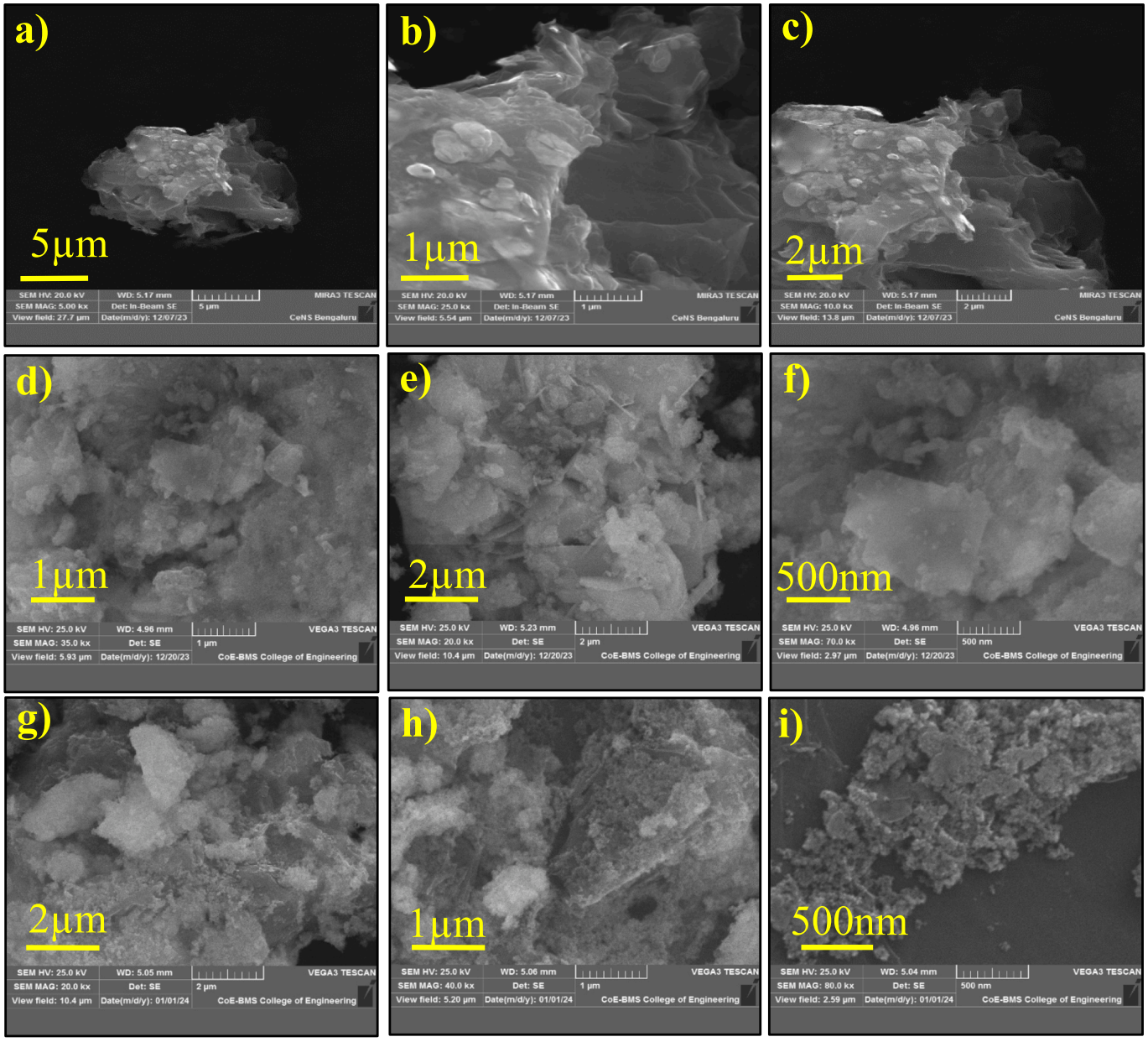

Fig. 2. SEM monographs of a-c) CeS, d-f) CeV, and g-i) CeV/CeS.

nitrogen gas. Light was illuminated and stirred the solution continuously. The formed bubbles were collected and examined using a thermal detector in gas chromatography.

The photoelectrochemical H_2 evolution was conducted in three electrode system consisting of Ag/AgCl (reference), Pt (counter) and FTO coated with catalysts as working electrode. Light source used was 300 W Xe lamp. The container was purged with nitrogen prior to the commencement of the reaction. The evolved H_2 was generated hydrogen was measured using a gas chromatograph.

2.4. Characterization

To get the structural properties of synthesized catalysts, XRD equipment (Brukner D2phaser) with Cu-Kα radiation was used. SEM images were recorded using JEOL JSM 840 A (5 kV acceleration voltage). JEOL/JEM 2100 (200 kV acceleration voltage) was used to record TEM pictures. The photoluminescence were carried out using RF-6000 spectroflurometer. The N_2 adsorption/desorption isotherm and pores size distribution were analyzed using Quanta chrome Autosorb 1C BET Surface Area & Pore Volume Analyzer. Photoelectrochemical properties were examined using a CHI 660D electrochemical workstation consisting of Ag/AgCl (reference) and Pt wire (counter) electrodes. Synthesized catalysts (15 mg) were sonicated in 0.5% Nafion solution and used to fabricate working electrode. 20 µL of the suspension was dropcasted, dried and evaluated electrochemical impedance investigations, photocurrent and Mott-Schottky plots.

3. Results and discussion

The XRD pattern of pure CeV, CeS, and CeV/CeS is shown in Fig. 1a. The presence of prominent peaks correlates to the formation of tetragonal CeV and is confirmed by JCPDS: 12–0757. No peaks are observed for other contaminants like CeO_2 or V_2O_5. In agreement with the results reported in the literature [24]. The diffraction peaks at observed for CeV at 2θ, 18.23, 24.27, 30.60, 32.56, 34.70, 39.78, 43.86, 48.31, 49.89, 62.10, and 68.67° are indexed to the crystallographic planes (101),

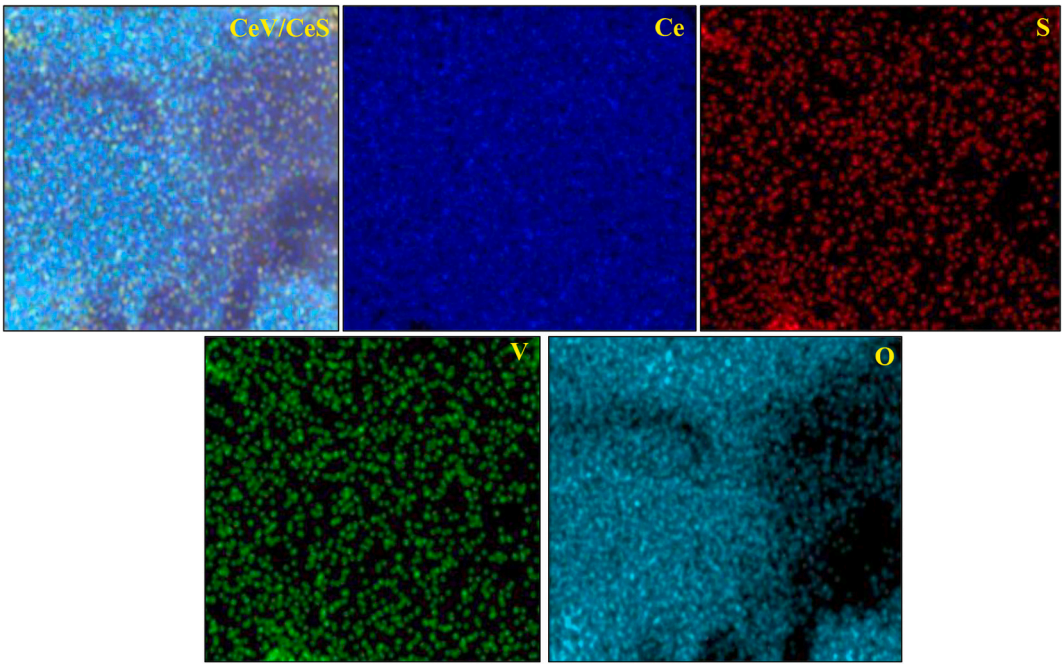

Fig. 3. EDX of CeV/CeS.

(200), (211), (112), (220), (202), (301), (103), (312), (400), (204), and (224). Lattice constants a = b = 7.383 Å and c = 6.485 Å indicate that the pattern is consistent with tetragonal type $CeVO_4$. The XRD of CeS consists of the lattice planes (211), (310), (321), (340), (420), (332), (431), and (441), which correspond to 2θ = 25.19, 32.51, 39.32, 47.09, 51.78, 58.21, and 61.79°. The diffraction peaks perfectly match the cubic-structured γ-CeS and are optimally referenced to JCPDS No. 50–0851 [29]. The XRD pattern of the CeV/CeS nanocomposite shows that both CeV and CeS planes are present. The overlap of peaks at similar positions makes distinguished peaks almost invisible. The presence of several distinct peaks at 2θ 18.23° (CeV) and 47.1° (CeS) in the composite indicates the formation of heterostructure. There are no peaks indicating impurities, and the diffraction peaks show that the material is crystallized. The crystallographic orientation and preferred direction of growth of the synthesized materials were further studied using the Material Studio software package. Fig. 1b shows the crystalline phases of CeV, CeS and CeV/CeS. Tetragonal $CeVO_4$ with I41/amd space group shows the bonding of Ce^{3+} in 8-coordinate geometry to 8 O^{2-} atoms. Four Ce—O bonds were found to be shorter (2.38 Å) than the other four (2.49 Å). The bond length of V—O is 1.77 Å. O^{2-} is bonded in a 3-coordinate geometry with two equivalent Ce^{3+} and one V^{5+} atom. Ce_2S_3 crystallizes in the tetragonal I42d space group. There are three inequivalent Ce^{3+} sites. In the first Ce^{3+} site, Ce^{3+} is bonded in 8-coordinate geometry to eight S^{2-} atoms. Ce—S bond length range is found to be 2.82–3.16 Å. In the second Ce^{3+} site, Ce^{3+} is bonded to eight S^{2-} atoms to form a mixture of distorted edge, face, and corner-sharing CeS_8 hexagonal bipyramids. In this case, the bond length of Ce—S ranges from 2.84 to 3.02 Å. In the third Ce^{3+} site, Ce^{3+} is bonded to eight S^{2-}. The Ce—S bond length is found to be 2.86–3.08 Å. There are three inequivalent S^{2-} sites. The first, second, and third S^{2-}sites site bound in 6-coordinate geometry to 6, 5 and 5 Ce^{3+} atoms, respectively, to form a mixture of distorted edge, face, and corner-sharing SCe_5 square pyramids.

Figure 2(a-i) shows SEM micrographs of the CeS, CeV, and CeV/CeS materials. In Fig. 2(a-c), the layered structure of CeS is depicted as a homogeneous sheet-like morphology, while in Fig. 2(d-f), the morphology of CeV is shown as more like small particles in aggregated structure. The CeV/CeS heterostructure (Fig. 2g-i) showed lobate-shaped particles growing on CeS sheets and also appeared like spherical particles embedded in the matrix, filling the sheet-like morphology entirely. Fig. 3 presents the EDX of the CeV/CeS, demonstrating the uniform and homogenous distribution of the elements. The findings also show that Ce, V, O, and S are present, confirming that the CeV/CeS is pure. The TEM images of CeS, CeV, and the CeV/CeS heterostructure further illustrate the morphology and provide further details. Fig. 4 (a&b) shows that the synthesized CeS had a sheet-like shape with many irregularly stacked structures which is further confirmed by TEM images at different magnification (Fig. S1). The discoidal shape of CeV is shown in the TEM micrograph (Fig. 4c&d). However, as can be seen in Figs. 4e&f, CeV/CeS heterostructure consists of evenly dispersed exfoliated sheets containing CeV particles.

The surface electronic state and elemental composition of CeV/CeS were studied in more detail by using XPS analysis, as shown in Fig. 5a. According to the survey spectra, CeV/CeS is composed of four main elements: Ce, V, O, and S. The high-resolution Ce 3d spectra (Fig. 5b) revealed the spin-orbit coupling of Ce $3d_{5/2}$ and Ce $3d_{3/2}$, with each peak splitting into multiple peaks. While the peaks centered at 900.21, 902.62, 907.05, and 916.53 eV (marked as *) are attributed to Ce $3d_{3/2}$, the peaks at 881.89, 885.21, 889.31, and 897.91 eV (marked as $^{\#}$) are associated with the binding energy of Ce $3d_{5/2}$. Since the Ce $3d_{5/2}$ and $3d_{5/2}$ bonding energies were present, it follows that the sample possesses Ce^{4+} and Ce^{3+} valence states [19]. The peaks at 517.35 and 524.45 eV, attributed to the spin-orbit coupling of $2p_{3/2}$ and $2p_{1/2}$, respectively, in the core level V 2p spectrum (Fig. 5c), indicate the presence of V^{5+}. The peak at 530.87 eV and another peak at 532.63 eV in the O 1 s deconvoluted spectrum (Fig. 5d) are attributed to the Ce-O-V bond and the presence of absorbed hydroxyl groups on the surface, respectively. Fig. 5e shows that the S 2p high-resolution spectra consist of two peaks at 163.91 and 161.59 eV (possibly due to the Ce—S bond) that are attributed to S $2p_{1/2}$ and S $2p_{3/2}$, respectively.

The photocatalytic performance CeV, CeS and CeV/CeS are significantly influenced by its specific surface area and pore-size volume. The N_2 adsorption/desorption isotherms for the synthesized materials are displayed in Fig. S2a, with the corresponding pore-size distribution curves shown in Fig. S2b. Notably, the BET surface area of CeS, CeV and CeV/CeS are found to be 46, 62 and 104 $m^2\ g^{-1}$ with corresponding pore size of 2.28, 1.97 and 3.46 nm, respectively. The enhanced photocatalytic hydrogen evolution in CeV/CeS could be attributed to the

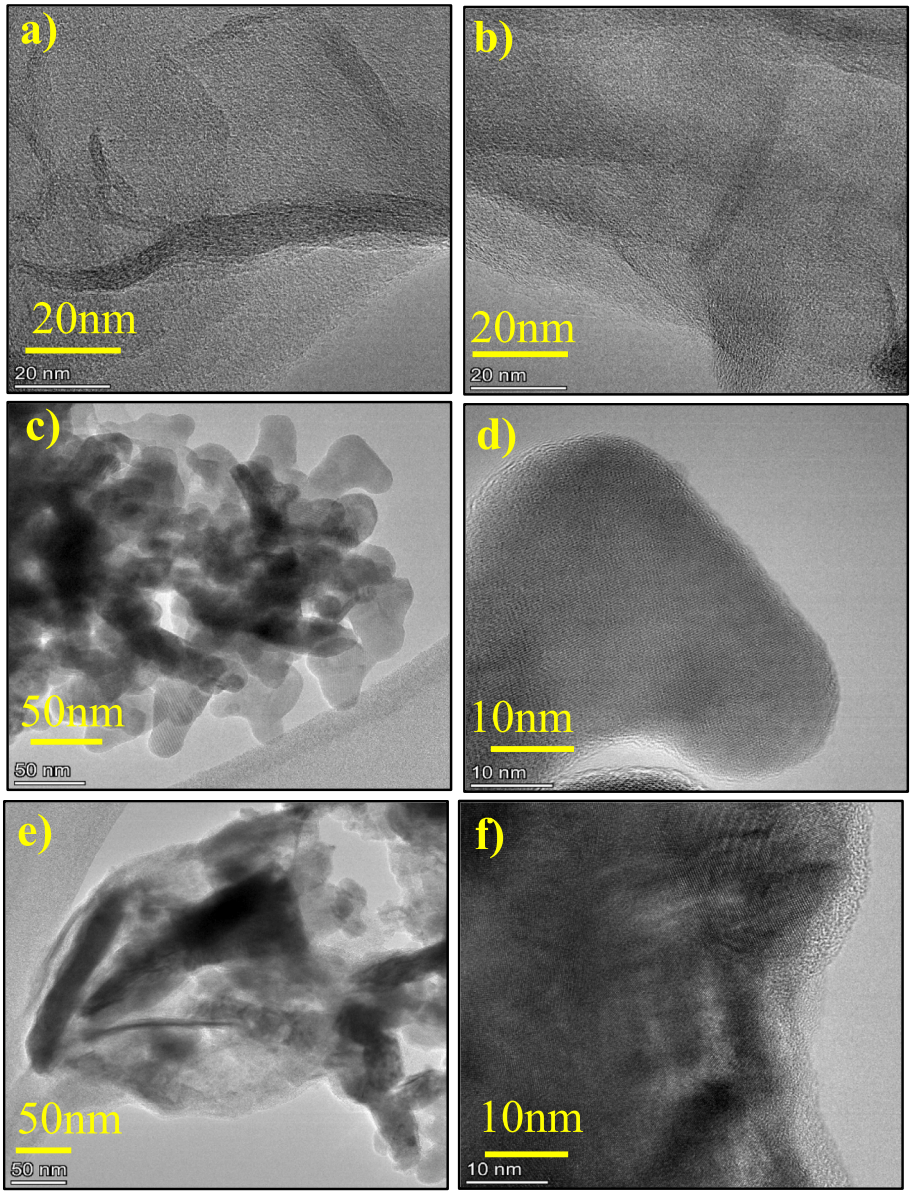

Fig. 4. TEM monographs of a&b) CeS, c&d) CeV, and e&f) CeV/CeS.

presence of abundant micro-sized pores, indicating the development of a distinctive surface structure.

3.1.1. *Optical and photo/electrochemical characterizations*

Synthesized materials were evaluated for their capacity to absorb ultraviolet and visible light and the obtained UV-DRS spectra are given in Fig. 6a. The absorption spectrum of CeV shows good capability both in the UV and visible regions, with an absorption edge at around 540 nm. The low-bandgap CeS showed superior light absorption ability, with the absorption edge at ~600 nm. Upon combining CeV and CeS in the CeV/CeS heterostructure, there was a blueshift and a redshift with respect to CeS and CeV, respectively, and the absorption edge was at around 585 nm. This combined effect in CeV/CeS could be due to the formation of heterostructures through interface and synergistic effects. The corresponding bandgap of the materials was found using the Kubelkan-Munk factor plot, as shown in Fig. 6b [32]. The bandgaps of CeV, CeS and CeV/CeS were found to be 2.41, 2.02 and 2.26 eV, respectively. Though the bandgap is increased in CeV/CeS with respect to CeS it is expected to have superior photocatalytic efficiency due to the decreased recombination of charge carriers. The photoluminescence (PL) spectra of the samples are depicted in Fig. 6c. The spectra show that the intensity of the peak is high in CeS, with a slight decrease in intensity observed in CeV. A significant decrease in intensity is observed in CeV/CeS heterostructure due to the quenching and trapping of charge carriers. The decreased intensity in CeV/CeS leads to the separation of charge carriers and hence expected to show efficient photocatalytic activities. The charge transfer resistance of the materials was examined using electrochemical impedance spectroscopy (EIS). The Nyquist plot in Fig. 6d indicates the lower charge transfer resistance in CeV/CeS compared to pristine CeV and CeS suggests interfacial electron transfer. To find out the flat band potential of the materials, Mott-Schottky plots were examined, as shown in Fig. 6e. The conduction band edge potentials (E_{CB}) of CeS, CeV and CeV/CeS were found to be −0.28, −1.19, and − 0.77 V, respectively. By using the E_{CB} and bandgap of the materials, the valence band edge potential (E_{VB}) could be easily estimated by considering the $Eg = E_{VB}\text{-}E_{CB}$ formula. CeV/CeS conduction band potential is found in between the pristine CeV and CeS indicating the interaction of CeV and CeS through

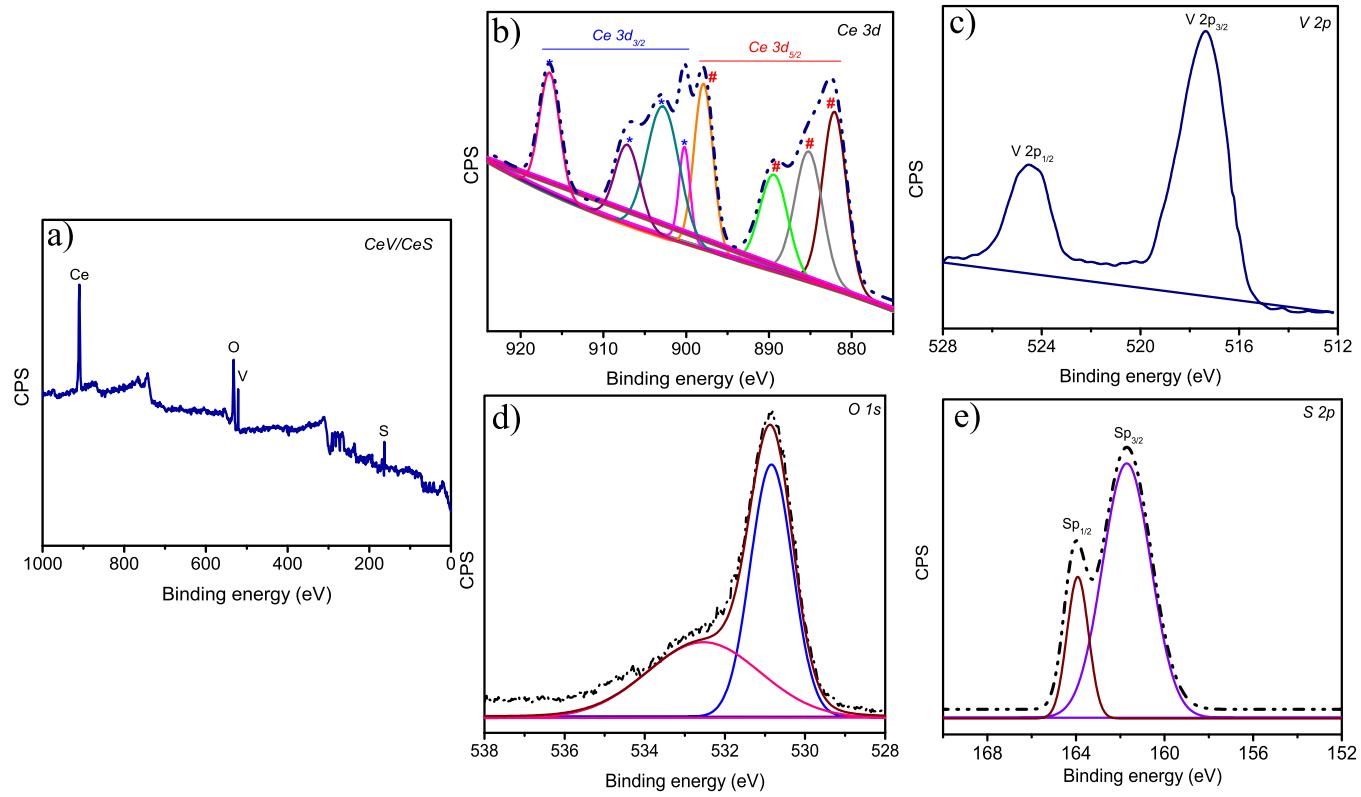

Fig. 5. XPS of CeV/CeS, a) Survey spectrum, b) Ce 3d, c) V 2p, d) O 1 s and e) S 2p.

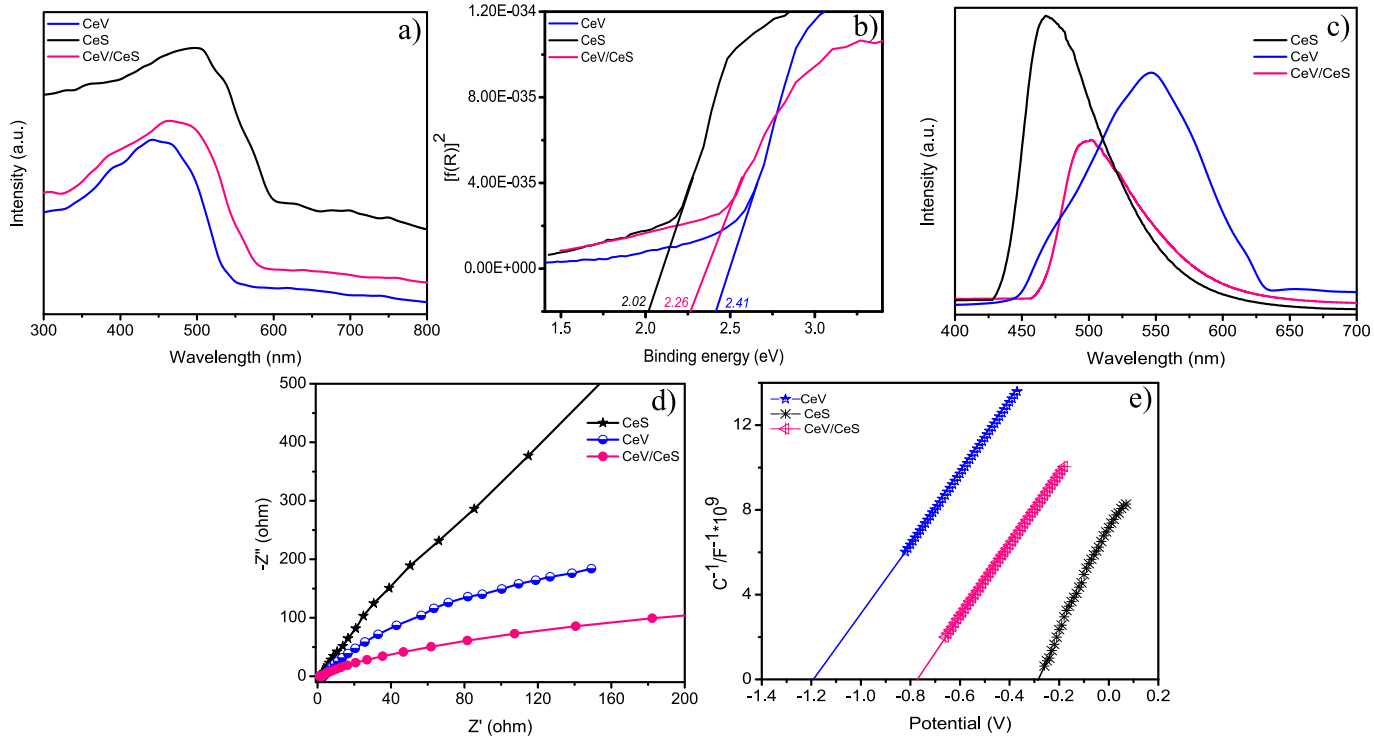

Fig. 6. CeV, CeS and CeV/CeS's a) UV-DRS spectra, b) Kubelka-Munk curves, c) Photoluminescence spectra, d) EIS analysis and e) Mott–Schottky plots.

the interface.

3.1.2. *Photochemical hydrogen evolution*

Photochemical hydrogen evolution tests were conducted continuously for 4 h under different instances and the results are given in Fig. 7a. There is no evolution of hydrogen in the absence of light, catalysts, and sacrificial agents, which indicates the prominence of individuals. A sacrificial agent is one that oxidizes easily than water and

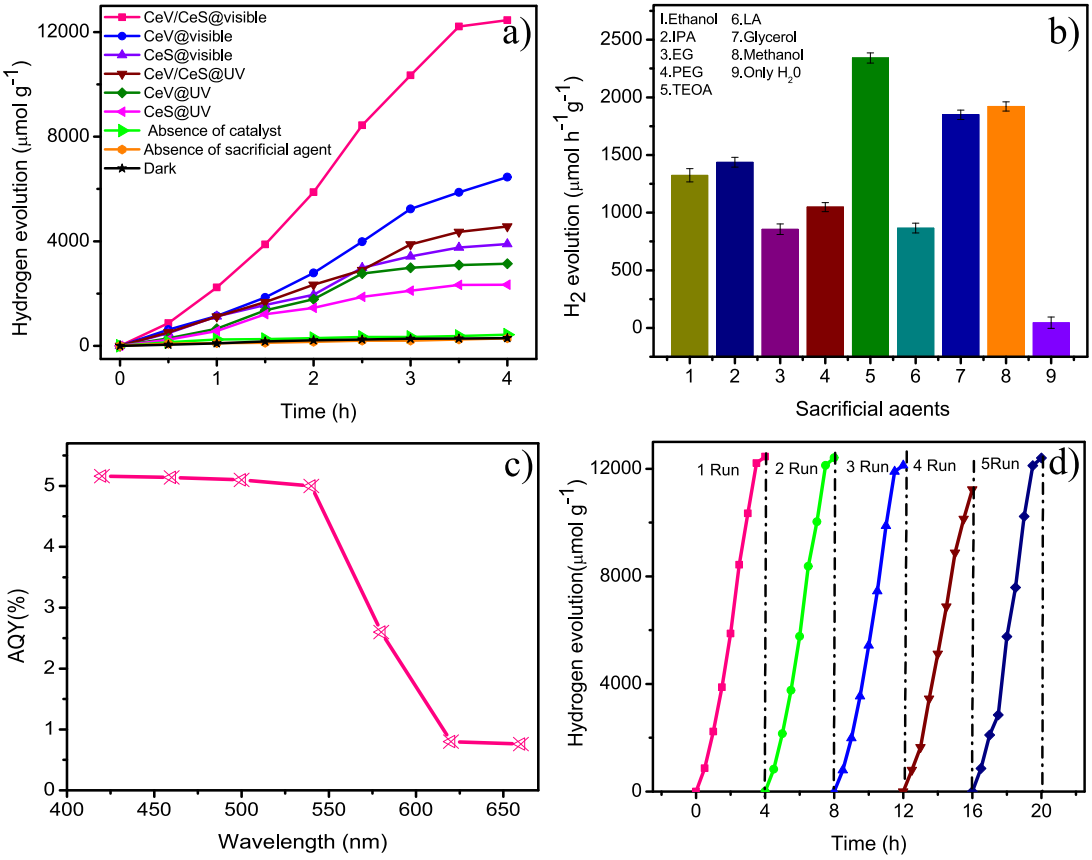

Fig. 7. a) Hydrogen evolution under different conditions, b) Effect of sacrificial agents, c) AQY of CeV/CeS and d) Stability studies of CeV/CeS.

Table 1
Hydrogen evolution under different conditions.

Sl. No.	Material and condition	H_2 evolution, μmol
1	CeV/CeS@visible	12,456
2	CeV@visible	6453
3	CeS@visible	3897
4	CeV/CeS@UV	4567
5	CeV@UV	3145
6	CeS@UV	2342

donates electrons for the reduction of holes. The results depicted in Table 1 indicate that all the materials are capable of undergoing photoredox reactions and evolving hydrogen. But obvious variation in their ability to evolve H_2 is observed due to variation in the structure, light irradiation, bandgap and defects. CeS is the one that showed low ability compared to other catalysts in the presence of both UV and visible light, probably due to the swift recombination of electrons and holes. CeV ability to evolve H_2 is high compared to CeS which managed to evolve 3145 and 6453 μmol under UV and visible light, respectively. Due to the formation of heterostructure, synergism, and effective separation of photo-induced electrons and holes, an enhanced H_2 evolution is observed in CeV/CeS. The H_2 evolution is favoured better under visible light than UV light and suggests the ability to absorb more photons in the visible region.

As observed, sacrificial agents play a prominent role in light-driven H_2 evolution. Hence, it is much needed to select a suitable sacrificial agent for H_2 evolution to achieve maximum activity in the presence of CeV/CeS. As observed in Fig. 7b, there is no activity in the presence of only water towards H_2 evolution, which suggests the need for a sacrificial agent during the reaction. Ethanol, isopropyl alcohol (IPA), ethylene glycol (EG), polyethylene glycol (PEG) and lactic acid (LA) showed moderate activity towards H_2 evolution. Glycerol and methanol showed comparatively high activity. TEOA showed maximum activity compared to all other sacrificial agents. The superior activity in the

Table 2
Comparison of the present work with related reports.

Sl No.	Material	Sacrificial agent	Light source	H_2 evolution	Ref.
1	SmV/S-C_3N_4	TEOA	400 W Xe light	22,618 μmol g^{-1}	[18]
2	$LaVO_4$/CN	10 ml of FFA or TEOA	The xenon lamp (300 W, 250 mW cm − 2) stimulated sunlight	0.95 mmol g^{-1}	[33]
3	CN/GdV	Methanol	300 W Xe lamp light intensity = 85 mW/cm^2, with filter λ > 400 nm	16,234 μmol g^{-1}	[34]
4	CdV/ZnV	Methanol	350 W Xenon lamp, 420 nm, 180 mW cm^{-2}	366.34 μmol h^{-1} g^{-1}	[35]
5	g-C_3N_4/$ZnIn_2S_4$	10% lactic acid	300 W Xe lamp, λ > 420 nm	10.92 mmol h^{-1} g^{-1}	[36]
6	$ZnCo_2S_4$/TiO_2	TEOA	300 W, Xe lamo, 420 nm cut off filter light	5580 μmol h^{-1} g^{-1}	[37]
7	$ZnIn_2S_4$/TiO_2	–	420 nm, visible	214.9 μmol g^{-1} h^{-1}	[38]
8	**CeV/CeS**	**TEOA**	**300 W Xe lamp (95 mW/cm^2) as a visible light source**	**2342 μmol g^{-1} h^{-1}**	**Present work**

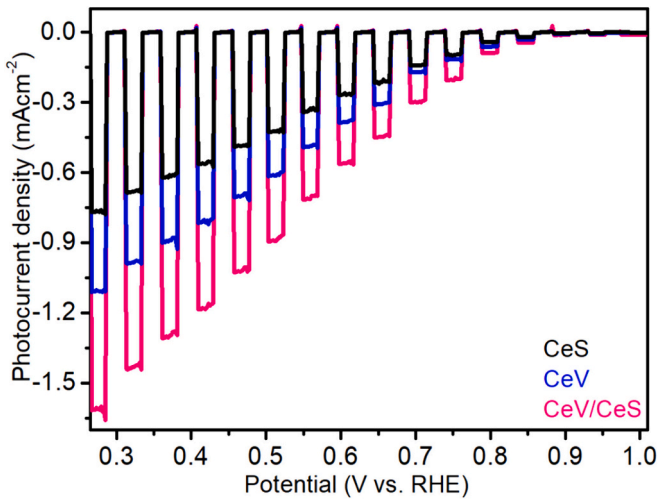

Fig. 8. Photoelectrochemical H_2 evolution.

TEOA and water systems could be attributed to the presence of multiple hydroxyl groups that allow facile electron mobility minimized byproducts due to low-side reactions. Fast reaction kinetics and uniform distribution in the water system ensure effective H_2 evolution compared to other sacrificial agents. The apparent quantum yield (AQYs) of CeV/CeS was assessed using eq. (1) and found to be 5.16% (Fig. 7c), pointing to its good stability in the visible region.

$$\mathrm{AQY}(\%) = 2 \times \frac{\text{The No.of } H_2 \text{ evolved}}{\text{The No.of incident photons}} \times 100 \quad (1)$$

The practical applicability of the catalysts depends on their reusability. Hence, a stability study was performed for CeV/CeS under optimum conditions (Fig. 7d). The CeV/CeS showed good stability for the first three runs. A decline in hydrogen evolution is observed at the fourth cycle, probably due to the decreased concentration of the sacrificial agent. A fresh sacrificial agent was added after the fourth cycle and found to evolve almost the same amount of H_2 as compared to the first run. The results of CeV/CeS for photochemical hydrogen evolution is good and found be superior over many reported methods as observed in Table 2. Furthermore, the diffraction peaks of XRD pattern of the CeV/CeS were hardly changed before and after the photocatalysis test (Fig. S3a), which suggested that the CeV/CeS has a relatively stable structure. SEM images (Fig. S3b) revealed that the morphology of the CeV/CeS has changed slightly from the first cycle to the fifth cycle while the composite showed aggregation on the surface.

3.1.3. *Photoelectrochemical H_2 evolution*

In the present investigation, we also examined the potential of CeS, CeV, and CeV/CeS films deposited over FTO for their light harnessing and charge separation properties by conducting photoelectrochemical experiments. Fig. 8 shows an evaluation of the current density-voltage (J-V) plots acquired from an optimized CeS, CeV, and CeV/CeS composite electrodes with respect to the applied potential under chopped light irradiation. The results indicate that the heterostructure improved photocurrent over the entire scanned potential range while maintaining a good photocurrent onset potential of +0.9 V vs. RHE. The CeV/CeS heterostructure has shown high photocurrent density at 0.25 V vs. RHE, which is almost 1.47 folds greater than that of CeV and 2.1 times that of CeS. It should be mentioned that the photocurrent density of −0.57 mA cm^{-2} was achieved in the present work at an applied voltage of +0.6 V vs. RHE, whereas CeV and CeS have shown −0.38 mA cm^{-2} and -0.33 mA cm^{-2} at the same applied potential. The increase in photocurrent density for CeV/CeS photocathodes indicates that the photocurrent improvement was due to supplementary photophysical reactions, in addition to the effective charge carrier separation and improved lifetime of these charge carriers.

3.1.4. *Mechanistic investigation*

Optical and electrochemical characterizations were used to predict the photocatalytic mechanism. Mott-Schottky results indicate positive slopes for all three synthesized catalysts and hence they are all n-type semiconductors. Theoretical flat band potentials for n-type semiconductors are considered +0.1 to the experimentally obtained E_{CB}. The E_{CB} of CeV, CeS, and CeV/CeS shows its ability to evolve hydrogen through water splitting since they possess negative potentials. The experimental results show the ability of CeS and CeV to individually evolve hydrogen since both of them are visible active materials. However, the faster recombination of photo-excited electrons and holes results in a lower efficiency. Upon combining the same amount of CeV and CeS, it has led to the formation of a heterostructure as shown in Fig. 9. The staggered band structure in CeV/CeS indicates that the charge carriers flow opposite to each other minimizing the carrier recombination. The type-II heterojunction with epitaxial junctions between two different semiconductors exhibits additional advantages such as ultrafast photoinduced charge separation. The electrons generated in the CB of the heterostructure lie more positive than the potential of oxygen reduction and hence it follows type-II mechanism. At, first, the CeV/CeS

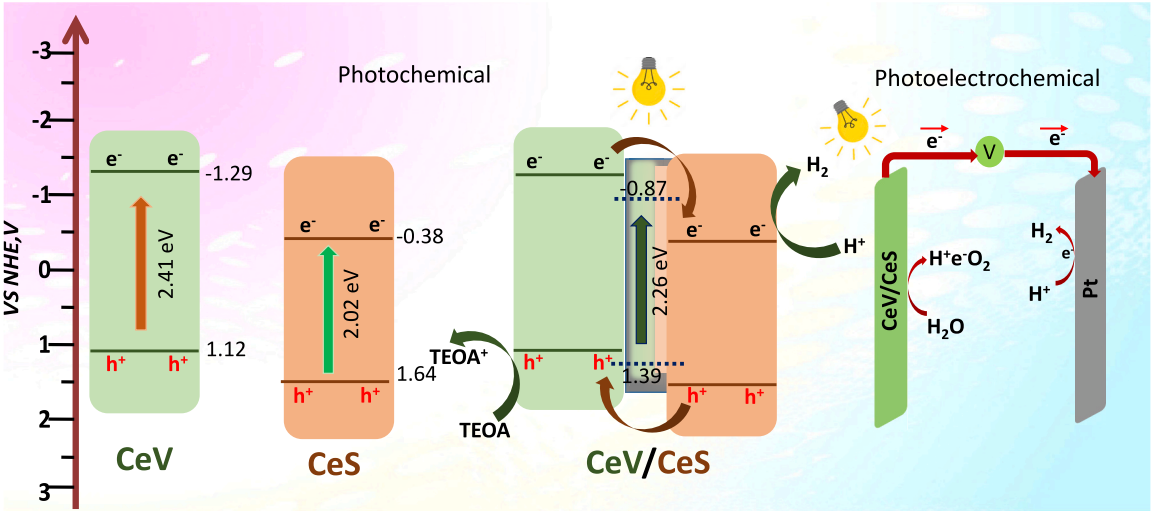

Fig. 9. Photocatalytic mechanism.

heterostructure is illuminated with light consisting of the TEOA/water system. A CeV undergoes excitation and liberates the electrons into the conduction band. On the other hand, the oxidation of TEOA significantly enhances electron liberation. The transfer of electrons from the conduction band of CeV to the conduction band of CeS occurs. The electrons in CeS exclusively generate hydrogen by reducing H^+ ions. This bandgap alignment and edge potential positions of CeV and CeS follow type-II heterostructure through staggered band alignment. The holes in the valence band of CeS show a tendency to move towards the valence band of CeV and speed up the oxidation of the sacrificial agent. This tailored type-II heterostructure, which separates the charge carriers, could be the reason for the enhanced photocatalytic activity in CeV/CeS.

4. Conclusions

A simple hydrothermal method has been developed for the synthesis of the CeV, CeS and CeV/CeS heterostructure. The synthesized materials showed profound structural and morphological characterizations. The layered CeS supported the growth of CeV through heterojunction. All three catalysts showed their ability to absorb light in both UV and visible regions. Enhanced light-driven activity was observed in CeV/CeS due to the formation of heterostructures of type-II nature. The lower PL intensity, enhanced surface area and lower charge transfer resistance show that CeV/CeS has better activity because photo-excited electrons and holes are efficiently separated. We found the hydrogen evolution in the presence of visible light and CeV/CeS to be high and comparable with many other previous reports. It is found that TEOA exhibited more activity to evolve hydrogen in the presence of CeV/CeS than other sacrificial agents under examination. Easy synthesis of CeV/CeS, its photocatalytic nature with good stability are the key features of the present work that motivate further research on metal vanadate-sulphide combinations.

CRediT authorship contribution statement

K. Yogesh Kumar: Writing – original draft, Methodology, Investigation, Formal analysis. **M.K. Prashanth:** Validation, Formal analysis, Data curation. **L. Parashuram:** Writing – original draft, Methodology, Investigation, Formal analysis. **H. Shanavaz:** Methodology, Investigation, Formal analysis, Data curation. **C.B. Pradeep Kumar:** Formal analysis, Data curation. **Fahd Alharethy:** Supervision, Software, Resources. **Byong-Hun Jeon:** Writing – original draft, Methodology, Investigation, Formal analysis. **K.K. Prashanth:** Validation, Formal analysis, Data curation. **M.S. Raghu:** Writing – review & editing, Visualization, Supervision, Conceptualization.

Declaration of competing interest

The authors declare that they have no known competing financial interests or personal relationships that could have appeared to influence the work reported in this paper.

Data availability

Data will be made available on request.

Acknowledgement

The authors are immensely elated and wish to express their indebted gratitude to the Management of the Faculty of Engineering and Technology, Jain University and NHCE for providing lab facilities. Authors extend their thanks and appreciation to Research Supporting Project (RSP2024R160) King Saud University, Riyadh, Saudi Arabia. This work was funded by the Korea Institute of Energy Technology Evaluation and Planning (KETEP) of the Republic of Korea (RS-2023-00255939).

Appendix A. Supplementary data

Supplementary data to this article can be found online at https://doi.org/10.1016/j.apcato.2024.206965.

References

[1] Q. Wang, K. Domen, Particulate Photocatalysts for light-driven water splitting: mechanisms, challenges, and design strategies, Chem. Rev. 120 (2019) 919–985, https://doi.org/10.1021/acs.chemrev.9b00201.
[2] N. Fajrina, M. Tahir, A critical review in strategies to improve photocatalytic water splitting towards hydrogen production, Int. J. Hydrog. Energy 44 (2019) 540–577, https://doi.org/10.1016/j.ijhydene.2018.10.200.
[3] L. Parashuram, M.K. Prashanth, P. Krishnaiah, C.B.P. Kumar, F.A. Alharti, K. Y. Kumar, B.-H. Jeon, M.S. Raghu, Nitrogen doped carbon spheres from Tamarindus indica shell decorated with vanadium pentoxide; photoelectrochemical water splitting, photochemical hydrogen evolution & degradation of bisphenol a, Chemosphere 287 (2022) 132348, https://doi.org/10.1016/j.chemosphere.2021.132348.
[4] S. Jia, Y. Su, B. Zhang, Z. Zhao, S. Li, Y. Zhang, P. Li, M. Xu, R. Ren, Few-layer MoS2 nanosheet-coated KNbO3 nanowire heterostructures: piezo-photocatalytic effect enhanced hydrogen production and organic pollutant degradation, Nanoscale 11 (2019) 7690–7700, https://doi.org/10.1039/c9nr00246d.
[5] S. Rao Akshatha, S. Sreenivasa, L. Parashuram, M.S. Raghu, K. Yogesh Kumar, T. Madhu Chakrapani Rao, Visible-light-induced photochemical hydrogen evolution and degradation of crystal violet dye by interwoven layered MoS2/Wurtzite ZnS Heterostructure Photocatalyst, ChemistrySelect 5 (2020) 6918–6926, https://doi.org/10.1002/slct.202001914.
[6] Z. Xie, Q. Liu, H. Zhao, H. Chen, G. Jia, E. Lei, C. Wang, Y. Zhou, Efficient hydrogen evolution from g-C3N4 under visible light by in situ loading Ag2Se nanoparticles as co-catalysts, Catal. Commun. 186 (2024) 106837, https://doi.org/10.1016/j.catcom.2023.106837.
[7] V. Navakoteswara Rao, N. Lakshmana Reddy, V. Preethi, M. Karthik, Y.-T. Yu, J. M. Yang, M. Mamatha Kumari, M.V. Shankar, A critical review on core/shell-based nanostructured photocatalysts for improved hydrogen generation, Int. J. Hydrog. Energy 48 (2023) 11754–11774, https://doi.org/10.1016/j.ijhydene.2023.01.059.
[8] S. Vadivel, P. Sujita, B. Paul, B. Vidhya, A. Sebastian, R. Selvarajan, Enhanced electrocatalytic HER performances of metal free SiC/g-C3N5 heterostructures, Catal. Commun. (2024) 106882, https://doi.org/10.1016/j.catcom.2024.106882.
[9] L.R. Nagappagari, T.D. Le, M.J. Ahemad, G.-J. Oh, G.-S. Shin, K. Lee, Y.-T. Yu, Enhancement of bifunctional photocatalytic activity of boron-doped g-C3N4/SnO2 heterojunction driven by plasmonic ag quantum dots, Mater. Today Nano. 22 (2023) 100325, https://doi.org/10.1016/j.mtnano.2023.100325.
[10] K.Y. Kumar, M.K. Prashanth, H. Shanavaz, L. Parashuram, F.A. Alharti, B.-H. Jeon, M.S. Raghu, Green and facile synthesis of strontium doped Nb2O5/RGO photocatalyst: efficacy towards H2 evolution, benzophenone-3 degradation and Cr (VI) reduction, Catal. Commun. 173 (2023) 106560, https://doi.org/10.1016/j.catcom.2022.106560.
[11] L.K. Babu, H.S. Rao, P.N.R. Kishore, N.L. Reddy, M.V. Shankar, Y.V.R. Reddy, UV–visible light sensitized NiCo2O4@g–C3N4 heterojunction: based nanocomposites as novel photocatalysts for enhanced hydrogen generation and electrochemical activity, J. Mater. Res. 3301–3315 (2023), https://doi.org/10.1557/s43578-023-01054-1.
[12] X. Zhang, S. Tong, D. Huang, Z. Liu, B. Shao, Q. Liang, T. Wu, Y. Pan, J. Huang, Y. Liu, M. Cheng, M. Chen, Recent advances of Zr based metal organic frameworks photocatalysis: energy production and environmental remediation, Coord. Chem. Rev. 448 (2021) 214177, https://doi.org/10.1016/j.ccr.2021.214177.
[13] S. Tian, H. Ren, Z. Liu, Z. Miao, L. Tian, J. Li, Y. Liu, S. Wei, P. Wang, ZnS/g-C3N4 heterojunction with Zn-vacancy for efficient hydrogen evolution in water splitting driven by visible light, Catal. Commun. 164 (2022) 106422, https://doi.org/10.1016/j.catcom.2022.106422.
[14] D. Liu, L. Wu, Z. Su, J. Liu, L. Feng, J. Huang, Sulfurized Ru constructed enhanced carrier separation heterojunction RuS_2/Bi_2WO_6 for high-efficiency photocatalytic hydrogen evolution, Catal. Commun. 183 (2023) 106760, https://doi.org/10.1016/j.catcom.2023.106760.
[15] S. Hamzad, K.Y. Kumar, M.K. Prashanth, D. Radhika, L. Parashuram, F.A. Alharti, B.H. Jeon, M.S. Raghu, Boron doped RGO from discharged dry cells decorated niobium pentoxide for enhanced visible light-induced hydrogen evolution and water decontamination, Surf. Interf. 36 (2023) 102544, https://doi.org/10.1016/j.surfin.2022.102544.
[16] A. Alsulami, Y.K. Kumarswamy, M.K. Prashanth, S. Hamzada, P. Lakshminarayana, C.B. Pradeep Kumar, B.-H. Jeon, M.S. Raghu, Fabrication of $FeVO_4$/RGO nanocomposite: an Amperometric probe for sensitive detection of methyl parathion in green beans and solar light-induced degradation, ACS Omega. 7 (2022) 45239–45252, https://doi.org/10.1021/acsomega.2c05729.
[17] X. Li, Z. Chen, Y. Yang, B. Lu, Y. Tang, J. Zhou, Recent progress and prospects of rare earth elements for advanced aqueous zinc batteries, inorganic chemistry, Frontiers 10 (2023) 5802–5811, https://doi.org/10.1039/d3qi01117h.
[18] A.S. Alkorbi, K.Y. Kumar, M.K. Prashanth, L. Parashuram, A. Abate, F.A. Alharti, B.-H. Jeon, M.S. Raghu, Samarium vanadate affixed sulfur self doped g-C3N4 heterojunction; photocatalytic, photoelectrocatalytic hydrogen evolution and dye degradation, Int. J. Hydrog. Energy 47 (2022) 12988–13003, https://doi.org/10.1016/j.ijhydene.2022.02.071.

[19] T. Kokulnathan, T. Sakthi Priya, T.-J. Wang, Surface engineering three-dimensional flowerlike cerium vanadate nanostructures used as Electrocatalysts: real time monitoring of Clioquinol in biological samples, ACS Sustain. Chem. Eng. 7 (2019) 16121–16130, https://doi.org/10.1021/acssuschemeng.9b02891.

[20] M. Chang, M. Wang, Y. Chen, M. Shu, Y. Zhao, B. Ding, Z. Hou, J. Lin, Self-assembled CeVO4/ag nanohybrid as photoconversion agents with enhanced solar-driven photocatalysis and NIR-responsive photothermal/photodynamic synergistic therapy performance, Nanoscale 11 (2019) 10129–10136, https://doi.org/10.1039/c9nr02412c.

[21] F.B. Li, X.Z. Li, M.F. Hou, K.W. Cheah, W.C.H. Choy, Enhanced photocatalytic activity of Ce3+–TiO2 for 2-mercaptobenzothiazole degradation in aqueous suspension for odour control, Appl. Catal. A Gen. 285 (2005) 181–189, https://doi.org/10.1016/j.apcata.2005.02.025.

[22] V. Ameri, M. Eghbali-Arani, S. Pourmasoud, New route for preparation of cerium vanadate nanoparticles with different morphology and investigation of optical and photocatalytic properties, J. Mater. Sci. Mater. Electron. 28 (2017) 18835–18841, https://doi.org/10.1007/s10854-017-7833-2.

[23] A. Zonarsaghar, M. Mousavi-Kamazani, S. Zinatloo-Ajabshir, Sonochemical synthesis of $CeVO_4$ nanoparticles for electrochemical hydrogen storage, Int. J. Hydrog. Energy 47 (2022) 5403–5417, https://doi.org/10.1016/j.ijhydene.2021.11.183.

[24] L. Gu, B. Feng, P. Xi, J. Xu, B. Chen, S. Zhong, W. Yang, Elucidating the role of Mo doping in enhancing the meta-xylene ammoxidation performance over the CeVO4 catalyst, Chem. Eng. J. 459 (2023) 141645, https://doi.org/10.1016/j.cej.2023.141645.

[25] L. Sun, X. Ye, Z. Cao, C. Zhang, C. Yao, C. Ni, X. Li, Upconversion enhanced photocatalytic conversion of lignin biomass into valuable product over CeVO4/palygorskite nanocomposite: effect of Gd3+ incorporation, Appl. Catal. A Gen. 648 (2022) 118923, https://doi.org/10.1016/j.apcata.2022.118923.

[26] F.A. Alharthi, A.E. Marghany, N.A.Y. Abduh, I. Hasan, Cerium vanadate with nitrogen doped reduced graphene oxide for visible light-driven hydrogen evolution and dye degradation, Phys. Status Solidi A 221 (2023), https://doi.org/10.1002/pssa.202300743.

[27] Q.Q. Liu, C.Y. Fan, H. Tang, T.D. Ma, J.Y. Shen, One-step synthesis of recycled 3D CeVO4/rGO composite aerogels for efficient degradation of organic dyes, RSC Adv. 6 (2016) 85779–85786, https://doi.org/10.1039/c6ra18013b.

[28] F. Xu, K. Meng, S. Cao, C.-H. Jiang, T. Chen, J. Xu, J. Yu, Step-by-Step Mechanism Insights into TiO_2/Ce_2S_3 S-Scheme Photocatalyst for Enhanced Aniline Production with Water as Proton Source, 2021, https://doi.org/10.21203/rs.3.rs-876600/v1.

[29] M.M. Rahman, J. Ahmed, A.M. Asiri, A glassy carbon electrode modified with γ-Ce_2S_3-decorated CNT nanocomposites for uric acid sensor development: a real sample analysis, RSC Adv. 7 (2017) 14649–14659, https://doi.org/10.1039/c6ra27414e.

[30] M. Ubaidullah, A.M. Al-Enizi, A. Nafady, S.F. Shaikh, K.Y. Kumar, M.K. Prashanth, L. Parashuram, B.-H. Jeon, M.S. Raghu, B. Pandit, Photocatalytic CO2 reduction and pesticide degradation over g-C_3N_4/Ce_2S3 heterojunction, J. Environ. Chem. Eng. 11 (2023) 109675, https://doi.org/10.1016/j.jece.2023.109675.

[31] H. Rauf, N. Yasmin, G. Ali, M.N. Ashiq, M. Safdar, M. Mirza, New insight in photocatalytic degradation of textile dyes over CeO_2/Ce_2S_3 composite, Phys. B Condens. Matter 632 (2022) 413760, https://doi.org/10.1016/j.physb.2022.413760.

[32] A. Biswas, C. Prathibha, Metal ion-intercalated layered hydrogen tri-titanate nanotubes: synthesis, characterization and their use in ultrafast and enhanced removal of hazardous contaminant fluoride from water, Mater. Adv. 3 (2022) 5947–5963.

[33] X. Li, J. Hu, T. Yang, X. Yang, J. Qu, C.M. Li, Efficient photocatalytic H2-evolution coupled with valuable furfural-production on exquisite 2D/2D LaVO4/g-C3N4 heterostructure, Nano Energy 92 (2022) 106714, https://doi.org/10.1016/j.nanoen.2021.106714.

[34] F.A. Alharthi, A. El Marghany, N.A.Y. Abduh, I. Hasan, Efficient light-driven hydrogen evolution and azo dye degradation over the GdVO4@g-C3N4 heterostructure, RSC Adv. 13 (2023) 20417–20429, https://doi.org/10.1039/d3ra02949b.

[35] I. Hasan, A. El Marghany, N.A.Y. Abduh, F.A. Alharthi, Efficient zinc vanadate Homojunction with cadmium nanostructures for photocatalytic water splitting and hydrogen evolution, Nanomaterials 14 (2024) 492, https://doi.org/10.3390/nano14060492.

[36] X. Dang, M. Xie, F. Dai, J. Guo, J. Liu, X. Lu, Ultrathin 2D/2D ZnIn2S4/g-C3N4 Nanosheet heterojunction with atomic-level intimate Interface for photocatalytic hydrogen evolution under visible light, Adv. Mater. Interfaces 8 (2021), https://doi.org/10.1002/admi.202100151.

[37] X. Dai, S. Feng, W. Wu, Y. Zhou, Z. Ye, X. Cao, Y. Wang, C. Yang, Photocatalytic hydrogen evolution and antibiotic degradation by S-scheme ZnCo2S4/TiO2, Int. J. Hydrog. Energy 47 (2022) 25104–25116, https://doi.org/10.1016/j.ijhydene.2022.05.269.

[38] G. Zuo, Y. Wang, W.L. Teo, Q. Xian, Y. Zhao, Direct Z-scheme TiO2–ZnIn2S4 nanoflowers for cocatalyst-free photocatalytic water splitting, Appl. Catal. B Environ. 291 (2021) 120126, https://doi.org/10.1016/j.apcatb.2021.120126.